modelling

MDPI

Article

Multi-Parameter Coupled Thermodynamic Analysis and Optimization of a Free-Piston Stirling Air Conditioner

Yajuan Wang [1,2,*], Yuehong Wang [1], Gao Zhang [1], Junde Guo [2] and Xiyao Liu [2]

[1] School of Intelligent Mechatronics, Shaanxi Energy Institute, Xianyang 712000, China
[2] School of Mechatronic Engineering, Xi'an Technological University, Xi'an 710021, China; gjd0119@163.com (J.G.)
* Correspondence: juanzia_2005@163.com

Abstract

To enhance the thermal performance of a Stirling air conditioner, this study applies Schmidt-based dimensionless analysis to systematically investigate the influence of key structural parameters on its cooling and heating characteristics. A dimensionless thermodynamic framework is established under the ideal isothermal assumptions of the Schmidt model to investigate the effects of temperature ratio, swept volume ratio, dead volume ratio, and phase angle on a Stirling system. The results indicate that increasing the temperature ratio enhances the thermodynamic driving potential; however, excessive temperature ratios introduce stronger irreversibilities, resulting in saturation or even degradation of effective cooling performance. The dimensionless cooling capacity increases significantly with phase angle, rising from 0.25 at $\alpha = 50°$ to 0.65 at $\alpha = 120°$, while heating capacity peaks at $\alpha \approx 71.6°$ with $\varepsilon_e = 0.18$. The *p*–*v* diagram analysis reveals optimal work output at $\alpha \approx 75°$, where the cycle area reaches 20.8, representing a 44.4% increase from the value at 15°. Performance saturation occurs at $\tau > 3$ and $\kappa > 6$ for cooling and beyond $\kappa > 4$ for heating. Within the assumptions of the ideal Schmidt model, the results suggest that medium-to-high temperature ratios ($\tau \approx 3$–4) combined with moderate swept volume ratios ($\kappa \approx 6$–8) provide the optimal balance between thermodynamic performance and structural compactness; these parameter combinations should be regarded as theoretical design references for ideal operating conditions rather than directly applicable engineering optimization guidelines.

Keywords: Stirling air conditioner; dimensionless capacity; phase angle; sweep volume; dead volume

1. Introduction

With the growing emphasis on energy conservation and environmental protection, there is an escalating demand for highly efficient and eco-friendly cooling technologies. Stirling air conditioning systems, featuring high thermal efficiency, ozone-friendly operation, low noise, and compact configurations, have emerged as a promising alternative to conventional compression-based cooling systems. These systems find broad applicability in aerospace, solar-driven cooling, and sustainable building environments. Distinct from traditional refrigeration systems [1,2], Stirling air conditioners [3,4] incorporate self-starting mechanisms [5] and regenerative cycles [6] and operate independently of refrigerants [7] and compressors, and thus providing a more sustainable and cleaner solution for cooling and heating applications [8,9]. These systems show potential in aerospace thermal control, solar-driven cooling, and energy-efficient building environments.

Check for updates

Academic Editor: Wei Gao

Received: 14 June 2026
Revised: 10 July 2026
Accepted: 17 July 2026
Published: 19 July 2026

Copyright: © 2026 by the authors. Licensee MDPI, Basel, Switzerland. This article is an open access article distributed under the terms and conditions of the Creative Commons Attribution (CC BY) license.

The thermodynamic performance of a Stirling air conditioner is governed by the coupled interaction among geometric configuration, operating conditions, and piston motion [10]. Key parameters, including the temperature ratio, swept volume ratio, dead volume ratio, and piston phase angle, directly influence pressure variation, heat transfer, and energy conversion throughout the Stirling cycle. Therefore, developing an accurate thermodynamic model capable of quantitatively evaluating the influence of these parameters is essential for structural optimization and performance improvement. To predict the thermodynamic behavior of Stirling systems, numerous analytical and numerical models have been developed. Among them, the classical Schmidt isothermal model remains one of the most widely adopted first-order analytical approaches because it provides closed-form solutions while preserving the essential thermodynamic characteristics of the Stirling cycle [11]. Based on the Schmidt theory, many researchers have investigated the effects of temperature ratio, phase angle, dead volume, and swept volume on output work and thermal efficiency [12]. Subsequently, semi-adiabatic models, finite-time thermodynamic models, and higher-order thermodynamic models were developed to account for irreversible heat transfer, pressure losses, and regenerator inefficiencies [13]. More recently, computational fluid dynamics (CFD), thermoacoustic simulation, and machine learning-assisted optimization have been employed to capture complex gas flow, transient heat transfer, and nonlinear transport phenomena within Stirling systems [14].

In addition to thermodynamic modeling, considerable effort has been devoted to improving the structural performance of Stirling systems. Regenerator optimization has received extensive attention through analytical solutions, CFD simulations, and experimental investigations, revealing the effects of porosity, thermal penetration depth, pressure loss, and heat transfer characteristics on system efficiency [15,16]. At the system level, thermodynamic–dynamic coupling models have been established to investigate the interaction between gas pressure, piston motion, damping, and vibration characteristics in free-piston Stirling devices. These studies have demonstrated that piston amplitude, phase angle, damping coefficient, and driving force significantly affect operating stability and thermodynamic performance [17]. Recent studies have further incorporated nonlinear driving strategies and experimental validation to improve the performance of low-temperature differential free-piston Stirling air conditioners under practical operating conditions. The present work focuses on revealing the thermodynamic mechanisms governing dimensionless cooling and heating performance rather than predicting the actual COP of practical air conditioning systems. The unique operating mechanism makes the thermodynamic performance particularly sensitive to interactions among the temperature ratio, swept volume ratio, dead volume ratio, and piston phase angle [18]. However, the combined effects of these parameters on both cooling and heating characteristics have not yet been comprehensively investigated within a unified dimensionless thermodynamic framework [19]. Furthermore, the FPSAC differs fundamentally from traditional crank-driven Stirling engines in that the piston and displacer motions are coupled through dynamic equilibrium between gas pressure and spring or gas stiffness rather than mechanical linkages [20–22].

Although these studies have considerably advanced the understanding of Stirling systems, several important limitations remain. First, most previous thermodynamic investigations primarily examined the influence of individual parameters independently, while the nonlinear coupling among multiple thermodynamic parameters has rarely been systematically quantified [23]. Second, existing studies generally focus on either cooling or heating performance, lacking a unified analytical framework capable of simultaneously evaluating both operating modes [24]. Third, high-fidelity CFD models, thermodynamic-dynamic coupling models, and experimental approaches provide high prediction accuracy but usually require considerable computational resources, detailed geometric information, and numerous empirical parameters, limiting their applicability during the preliminary design stage [25]. Consequently, a simple yet systematic analytical model that can rapidly evaluate the coupled effects of multiple design parameters remains desirable.

Motivated by the above-identified research gap, this work develops a Schmidt-based dimensionless thermodynamic modeling framework for a free-piston Stirling air conditioner to systematically investigate the coupled effects of multiple geometric and operating parameters on both cooling and heating performance. Unlike most existing studies, which primarily focus on the influence of a single parameter or evaluate system performance under fixed operating conditions, the proposed model reveals the nonlinear coupling mechanisms among temperature ratio, swept volume ratio, dead volume ratio, and piston phase angle within a unified analytical framework. Furthermore, dimensionless performance indices are introduced to enable direct comparison of cooling capacity, heating capacity, and cycle work under different parameter combinations, thereby identifying favorable operating regions under the assumptions of the ideal Schmidt model. The proposed modeling framework provides theoretical insight into multi-parameter thermodynamic interactions and offers a foundation for subsequent non-ideal thermodynamic modeling, dynamic coupling analysis, and engineering optimization of free-piston Stirling air conditioning systems.

The main contributions of this work are summarized as follows:

(1) A Schmidt-based dimensionless thermodynamic modeling framework is established for free-piston Stirling air conditioners.
(2) The coupled influences of temperature ratio, swept volume ratio, dead volume ratio, and piston phase angle on both cooling and heating performance are systematically quantified within a unified analytical framework.
(3) Dimensionless performance indices are employed to identify favorable parameter combinations and reveal the nonlinear coupling mechanisms among key design variables under ideal isothermal assumptions.
(4) The obtained results provide theoretical upper-bound references for preliminary parameter selection and lay the foundation for future non-ideal and coupled dynamic–thermodynamic analyses.

2. Dimensionless Analysis Based on the Schmidt Model

2.1. Working Principle

A free-piston Stirling air conditioning system can provide both cooling and heating functions; its main components include the expansion and compression chambers, a power piston, and a displacer, with piston motion generated by a linear oscillating motor. During heating, the compression chamber extracts thermal energy from the environment. Piston-induced compression increases the gas pressure, and the accumulated heat is transferred to the expansion chamber, which subsequently discharges it, thus absorbing heat on the cold side and rejecting it on the hot side, as shown in Figure 1a. During cooling, the compressed gas in the compression chamber directly releases heat to the surroundings; gas expansion in the expansion chamber draws heat from the environment. The cyclic compression–expansion process sustains heat uptake at the cold end and heat release at the hot end, producing refrigeration, as shown in Figure 1b. Figure 1c illustrates the ideal Stirling thermodynamic cycle on the p–v diagram. During the isothermal compression process (1–2), the working gas rejects heat to the surroundings, resulting in an increase in pressure while the cylinder volume decreases. Subsequently, during the constant-volume regenerative heat transfer process (2–3), the gas absorbs heat from the regenerator, leading to an increase in temperature with nearly unchanged volume. The isothermal expansion process (3–4) allows the gas to absorb heat from the low-temperature source while producing expansion work. Finally, during the constant-volume regenerative cooling process (4–1), the working gas transfers heat back to the regenerator, completing one thermodynamic cycle. This cyclic heat transfer mechanism enables the free-piston Stirling air conditioner to operate alternately in cooling and heating modes.

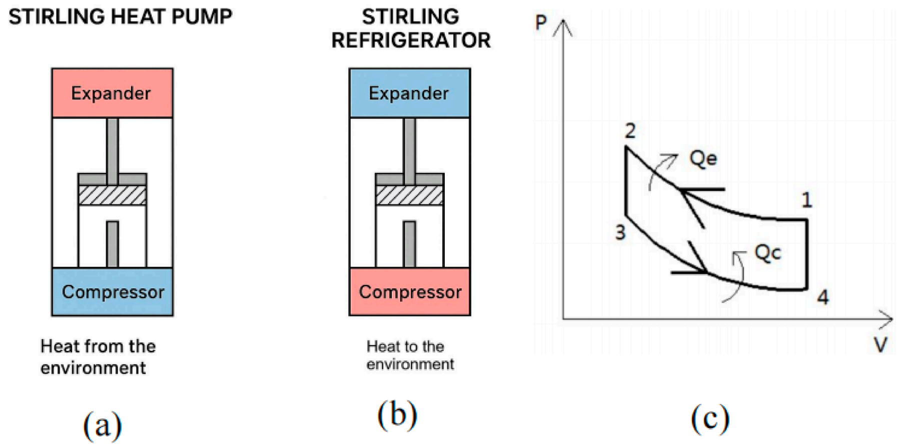

Figure 1. (**a**) Heating mode; (**b**) Cooling mode; (**c**) p–v diagram.

Based on the trigonometric relationships, the adjacent side is defined as $(1\text{–}\tau\text{–}\kappa\cos a_{\mathrm{dr}})$, the opposite side as $\kappa\sin\alpha_{dr}$, and the hypotenuse as the resultant side. Accordingly, the angle corresponding to $\kappa\sin\alpha_{dr}$ is denoted as θ_1, which is referred to as the pressure phase angle, as illustrated in Figure 2.

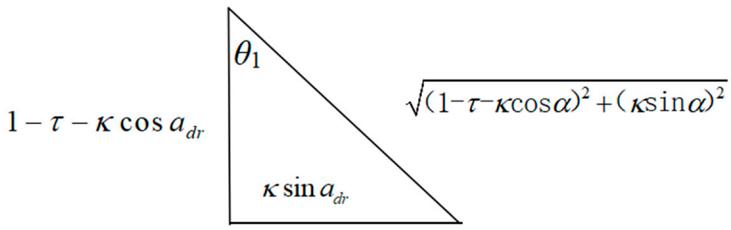

Figure 2. Parameters relationship of the FPSAC.

In practical free-piston systems, piston and displacer motions are governed by gas–spring–mass coupling, leading to deviations from ideal sinusoidal trajectories. To account for this effect, a phase-corrected harmonic representation is introduced in Equation (1):

$$x(t) = A\sin(\omega t + \varphi) + \delta(t) \tag{1}$$

2.2. Model Assumptions

For the dimensionless thermodynamic analysis based on the Schmidt model, several fundamental assumptions are introduced to reduce model complexity and enable analytical solutions [26]:

(1) The regeneration process is considered ideal, with a regenerator effectiveness of 100%.
(2) No pressure loss occurs within the system, and the gas pressure in all chambers is assumed to be equal at any instant.
(3) The working fluid behaves as an ideal gas and flows steadily within each thermodynamic chamber.
(4) The working fluid is perfectly sealed, and its total mass remains constant throughout the cycle.
(5) The volumes of the compression and expansion chambers vary sinusoidally with time.

(6) During the entire thermodynamic cycle, the temperatures of the working fluid in the cylinder, piston surfaces, and dead volume regions are assumed to be constant.
(7) The gas temperature in the regenerator is taken as the arithmetic mean of the expansion and compression chamber temperatures.

It should be emphasized that the present model is based on the classical Schmidt isothermal framework, which represents the idealized upper-bound performance of the system. In practical free-piston Stirling air conditioners, additional irreversibilities, including regenerator inefficiency, pressure drop, shuttle heat transfer, and gas leakage, play a significant role.

Therefore, the current analysis aims to reveal intrinsic thermodynamic trends and parameter-coupling mechanisms, rather than to provide direct quantitative predictions. The results obtained should be interpreted as theoretical limits, and further corrections are required for engineering applications.

2.3. Basic Equations and Analysis

To facilitate the derivation of the thermodynamic equations, the kinematic definitions adopted in the present study are illustrated in Figure 2. The expansion piston and compression piston perform sinusoidal reciprocating motions with a phase difference α. The instantaneous displacements are represented by $x_e(t)$ and $x_c(t)$, respectively, from which the instantaneous expansion volume V_e and compression volume V_c can be obtained. The total working volume is therefore expressed as the sum of the two chamber volumes.

The instantaneous expansion volume V_e, compression volume V_c, and total working volume V_T are defined as in Equation (2):

$$\begin{cases} V_\mathrm{e} = \frac{1}{2}V_E(1-\cos(2\pi ft)) \\ V_\mathrm{c} = \frac{1}{2}V_E(1+\cos(2\pi ft)) + \frac{1}{2}\kappa V_E[(1-\cos(2\pi ft - a)] \\ V_T = V_e + V_c \end{cases} \quad (2)$$

In this study, as illustrated in Figure 2, V_e and V_c denote the instantaneous volumes of the expansion and compression chambers, respectively, whereas V_T is the total working volume. The piston phase angle α defines the temporal difference between the expansion and compression piston motions, which determines the thermodynamic coupling during one operating cycle; t denotes the time measured from the top dead center of the expansion piston, and f is the system operating frequency. For the free-piston Stirling air conditioner, the motions of the expansion piston and compression piston are non-overlapping. When the minimum volume of the compression chamber approaches zero, the volume variation rate satisfies $\mathrm{d}V_c/\mathrm{dt} = 0$. Under this condition, $\sin(\omega t)$ can be expressed as shown in Equation (3):

By combining Equations (1) and (2), the expression for $\sin(\omega t)$ can be derived as shown in Equation (3):

$$\omega t = \tan^{-1}[(\kappa \sin a)/(\tau + \cos a + 1)] \quad (3)$$

Under the constraint of mass conservation, and assuming instantaneous pressure equilibrium throughout the system with constant temperatures in the compression and expansion chambers, the pressure p can be expressed as Equation (4):

$$p = \frac{K}{(1-\tau-\kappa\cos a)\cos(\omega t) - \kappa \sin a \sin(\omega t) + \tau + 1 + \kappa + 2s} \quad (4)$$

during which $s = 2\chi\tau/(\tau + 1)$.

From the above analysis, the expression for the pressure p can be written as shown in Equation (5):

$$p = \frac{K}{\sqrt{\tau^2 + 2(\tau - 1)\kappa\cos a + \kappa^2 - 2\tau + 1} \cdot \cos(\omega t + \theta_1) + \tau + \kappa + 1 + 2s} \tag{5}$$

Let $B = \sqrt{\tau^2 + 2(\tau - 1)\kappa\cos\alpha + \kappa^2 - 2\tau + 1}$, $S = \tau + \kappa + 2s + 1$, $c = B/S$;

The detailed derivation from Equation (2) to Equation (5) is provided in Appendix A to ensure mathematical transparency.

Consequently, Equation (5) can be rewritten as Equation (6):

$$p = K/(B(1 + \mathrm{c}\cos(\omega t + \theta_1)) \tag{6}$$

when $x = \pi - \theta_1$, the maximum pressure of the system, p_{max}, satisfies Equation (7):

$$p_{\max} = K/(B(1 - c)) \tag{7}$$

when $x = -\theta_1$, the minimum pressure of the system, p_{min}, satisfies Equation (8):

$$p_{\min} = K/(B(1 + c)) \tag{8}$$

The instantaneous pressure p can be expressed in terms of the maximum cycle pressure p_{max}, the minimum cycle pressure p_{min}, and the mean cycle pressure p_{mean} in Equation (9):

$$p = \begin{cases} p_{\min}(1 + c)/[1 + c \cdot \cos(\omega t + \theta_1)] \\ p_{\max}(1 - c)/[1 + c \cdot \cos(\omega t + \theta_1)] \\ p_{mean}\sqrt{1 - c^2}/[1 + c \cdot \cos(\omega t + \theta_1)] \end{cases} \tag{9}$$

The pressure ratio γ is defined as the ratio of the maximum pressure p_{max} to the minimum pressure p_{min} as shown in Equation (10):

$$\gamma = (1 + c)/(1 - c) \tag{10}$$

The heat absorbed by the expansion chamber Q_e, and the heat released by the compression chamber Q_c, are given by Equation (11):

$$\begin{cases} Q_e = \frac{P_{mean} V_E \pi \cdot c \cdot \sin\theta_1}{1 + \sqrt{1 - c^2}} \\ Q_c = -\tau Q_E \end{cases} \tag{11}$$

The cycle work W can be expressed as Equation (12):

$$W = \frac{p_{mean} V_{SE} \cdot \pi(1 - \tau) \cdot c \cdot \sin\theta_1}{1 + \sqrt{1 - c^2}} \tag{12}$$

The dimensionless work Z is defined as the ratio of cycle work to the reference pressure–volume product, representing the normalized work capacity per cycle. It should be noted that Z does not directly represent power output, as frequency effects are not included. The dimensionless work Z is defined as in Equation (13):

$$Z = W/p_{\max} V_T \tag{13}$$

where the total swept volume V_T is defined as the sum of the expansion chamber volume V_e and the compression chamber volume V_c.

https://doi.org/10.3390/modelling7040144

The coefficients of performance for cooling, COP_c, and heating, COP_h, are defined as shown in Equation (14):

$$\begin{cases} COP_h = \tau/(\tau-1) \\ COP_c = 1/(1-\tau) \end{cases} \tag{14}$$

The dimensionless cooling capacity ε_c and heating capacity ε_h are shown in Equation (15):

$$\begin{cases} \varepsilon_e = \frac{\tau\cdot\pi\cdot c\cdot\sin\varphi}{\left(1+\sqrt{1-c^2}\right)(\kappa+1)} \\ \varepsilon_c = \frac{\pi\cdot c\cdot\sin\varphi}{\left(1+\sqrt{1-c^2}\right)(\kappa+1)} \end{cases} \tag{15}$$

2.4. Dynamic Model of Free-Piston Motion

This section outlines the isothermal model analysis of a free-piston Stirling air conditioner system. Initially, the instantaneous volumes of the expansion chamber, compression chamber, and their total are defined.

Under the specific condition where the minimum volume of the compression chamber approaches zero, an expression for the sine of the crankshaft angle is derived. Based on the assumptions of mass conservation and constant chamber temperatures, a mathematical model for the instantaneous system pressure is established, introducing the concept of the pressure phase angle. Subsequently, the maximum and minimum pressures within the cycle are calculated, and the pressure ratio is defined. Based on these parameters, the system's heat absorption, heat rejection, and net cycle work are calculated, and the concept of dimensionless work is introduced. Finally, key performance indicators, including the coefficients of performance for cooling/heating and the dimensionless cooling/heating capacities, are defined, thereby completing the comprehensive theoretical derivation from fundamental kinematic relationships to overall system performance evaluation. The flow chart is shown in Figure 3 below.

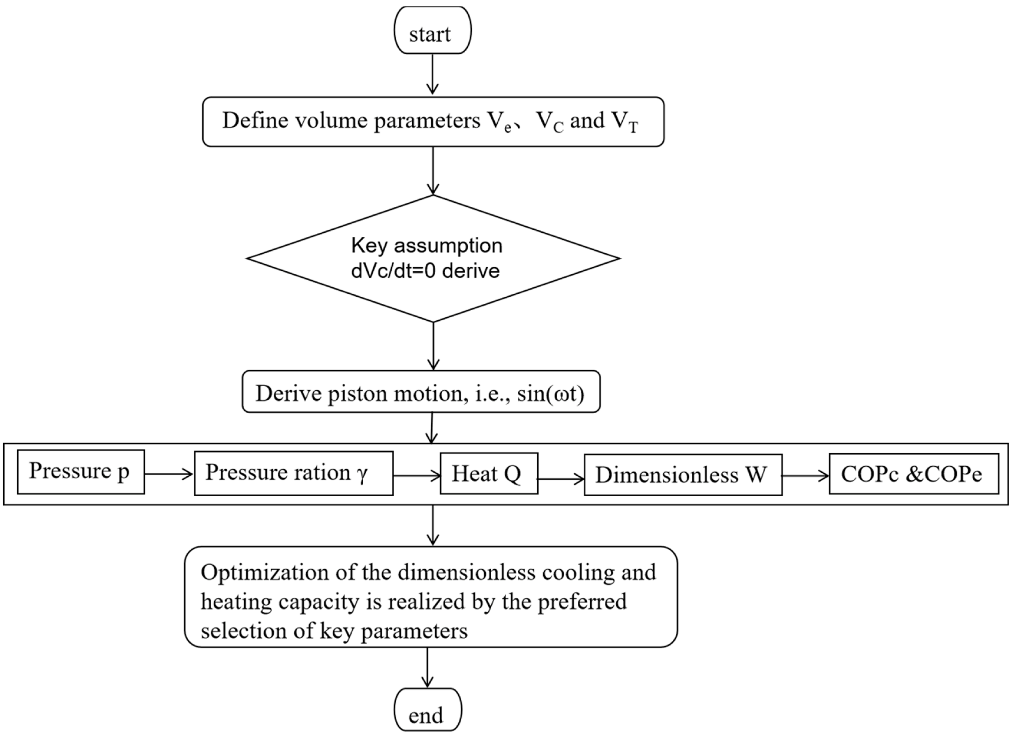

Figure 3. The flow chart.

3. Results and Discussion

3.1. Effect of Piston Phase Angle α and Swept Volume Ratio κ on the Dimensionless Capacity $\varepsilon_c/\varepsilon_h$

The analysis indicates that the dimensionless cooling capacity ε_c exhibits a pronounced nonlinear variation with the piston phase angle α and the swept volume ratio κ, revealing a complex coupling effect of these two structural parameters on the cooling performance. For small swept volume ratios ($\kappa < 2$), the dimensionless cooling capacity ε_c increases rapidly with the piston phase angle α, then levels off or slightly decreases beyond a certain angle. When $\kappa = 1$, ε_c increases from 0 to approximately 0.09 as α rises from 0 to 1.5. In contrast, for moderate to large κ values ($\kappa > 4$, particularly for $\kappa = 6$–8), the surface variation is smoother, indicating reduced sensitivity of the cooling performance to α. When α is small ($\alpha < 1$), ε_c exhibits significant growth; at larger α ($\alpha > 3$), however, the increase in ε_c remains limited even with higher κ (ranging from 4 to 8), demonstrating a saturation effect. The optimal cooling performance occurs in the region of moderate phase angles ($\alpha \approx 1.5$) and medium-to-high swept volume ratios ($\kappa \approx 6$). The surface forms a plateau in this region (ε_c stabilizes within the high range of 0.10 to 0.12), indicating that multiple parameter combinations can achieve near-optimal cooling performance, providing a certain degree of design redundancy (see Figure 4a).

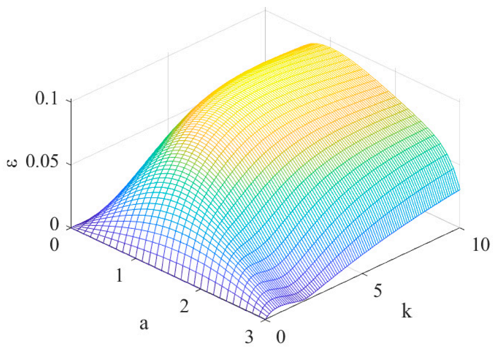

(**a**)

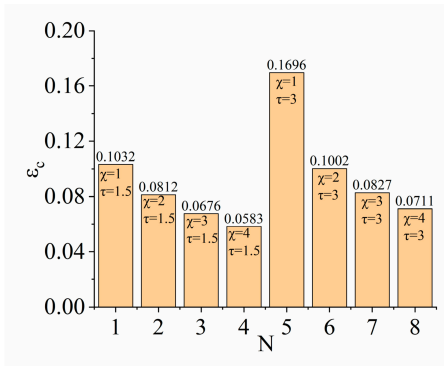

(**b**)

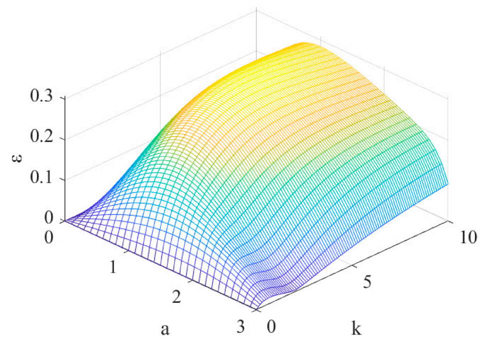

(**c**)

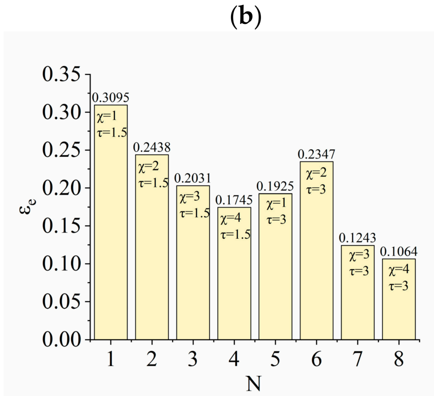

(**d**)

Figure 4. (**a**) $\chi = 1$, $\tau = 1.5$ (the cooling mode). (**b**) Dimensionless cooling capacity under varying dead volume and temperature ratio. (**c**) $\chi = 1$, $\tau = 1.5$ (the heating mode). (**d**) Dimensionless heating capacity under varying dead volume and temperature.

Under the same dead volume ratio, the cooling performance at a temperature ratio of $\tau = 3$ generally exceeds that at $\tau = 1.5$, which indicates that a higher temperature ratio, corresponding to a relatively higher hot-end temperature compared to the cold-end, enhances the system's thermal driving potential and thereby increases the cooling capacity. When $\tau = 3$, the ε_c values for $\chi = 1$, 2, 3, and 4 are 0.1696, 0.1002, 0.0827, and 0.0711, respectively, significantly exceeding the corresponding values of 0.1032, 0.0812, 0.0676, and 0.0583 at τ = 1.5. Under a fixed temperature ratio, the dimensionless cooling capacity ε_c decreases gradually as the dead volume ratio χ increases from 1 to 4, which indicates that larger dead volumes result in heat transfer delays during the reciprocating compression–expansion process and reduce volumetric utilization efficiency, thereby diminishing the cooling performance, When τ is 3, ε_c decreases from 0.1696 to 0.0711 as χ increases from 1 to 4; similarly, at τ = 1.5, it drops from 0.1032 to 0.0583, respectively. The dimensionless cooling capacity ε_c reaches its maximum (ε_c = 0.1696) when the dead volume ratio χ = 1 and the temperature ratio τ = 3, whereas the minimum value (ε_c = 0.0583) occurs at χ = 4 and τ = 1.5, as shown in Figure 4b.

The dimensionless heating capacity ε_h exhibits a similar dependence on the piston phase angle α and swept volume ratio κ as the cooling capacity. Therefore, only the distinctive characteristics of the heating mode are discussed below. The ε_h value is highest at χ = 1 (0.1696), decreases at χ = 2 (0.1002), and then shows a slight fluctuation (to 0.0827 at χ = 3 and 0.0711 at χ = 4), initially increases and then decreases with χ, indicating a non-monotonic effect of the temperature ratio on heating performance, as shown in Figure 4c.

The dimensionless heating capacity ε_h reaches its maximum at a dead volume ratio of χ = 1 and a temperature ratio of τ = 1.5, indicating that the optimal heating performance corresponds to a combination of low dead volume and low temperature ratio (see Figure 4d). It is noteworthy that while the maximum ε_h occurs at τ = 1.5, the absolute values of ε_h at τ = 3 are significantly higher across all χ values (e.g., 0.1696 vs. 0.1032 at χ = 1), suggesting a trade-off between the optimal operating point and overall performance magnitude dependent on the temperature ratio.

The optimal operating points differ between the cooling and heating modes: the cooling performance is maximized at a high temperature ratio and large swept volume, whereas the heating performance is optimized at a low temperature ratio with a large swept volume. Specifically, the maximum dimensionless cooling capacity of ε_c = 0.1696 is achieved at τ = 3 and χ = 1. In contrast, the optimal heating performance occurs under the condition of "low temperature difference and small dead volume", that is, at τ = 1.5 and χ = 1, where the dimensionless heating capacity ε_h = 0.1032 is the optimal value for the corresponding operating condition. The difference arises from the distinct thermodynamic cycle characteristics of the Stirling air conditioner in cooling and heating modes. In the cooling mode, work performed by the driving end circulates the gas under a high temperature difference, and a larger swept volume increases the absorbed heat, enhancing the cooling performance. In the heating mode, however, excessively high temperature differences reduce efficiency, so appropriately lowering the temperature difference can improve the heating performance coefficient.

3.2. Effect of Temperature Ratio τ and Swept Volume Ratio κ on Dimensionless Cooling Capacity ε_c/Heating Capacity ε_e

With the increase in swept volume ratio κ, the dimensionless cooling capacity ε_c exhibits a monotonic rise, indicating that enhanced sweeping capability improves cooling performance. When κ exceeds 6, the response surface tends to flatten, with ε_c values approaching an upper limit of around 0.2 under high temperature ratios (as illustrated in Figure 5a). The dimensionless cooling capacity increases monotonically with both the swept volume ratio κ and the temperature ratio τ. The performance enhancement is particularly significant when $\tau < 2$ and $\kappa < 6$. Beyond these ranges, however, the increase gradually diminishes and approaches a plateau, indicating that further enlargement of κ or τ provides limited additional cooling benefit.

https://doi.org/10.3390/modelling7040144

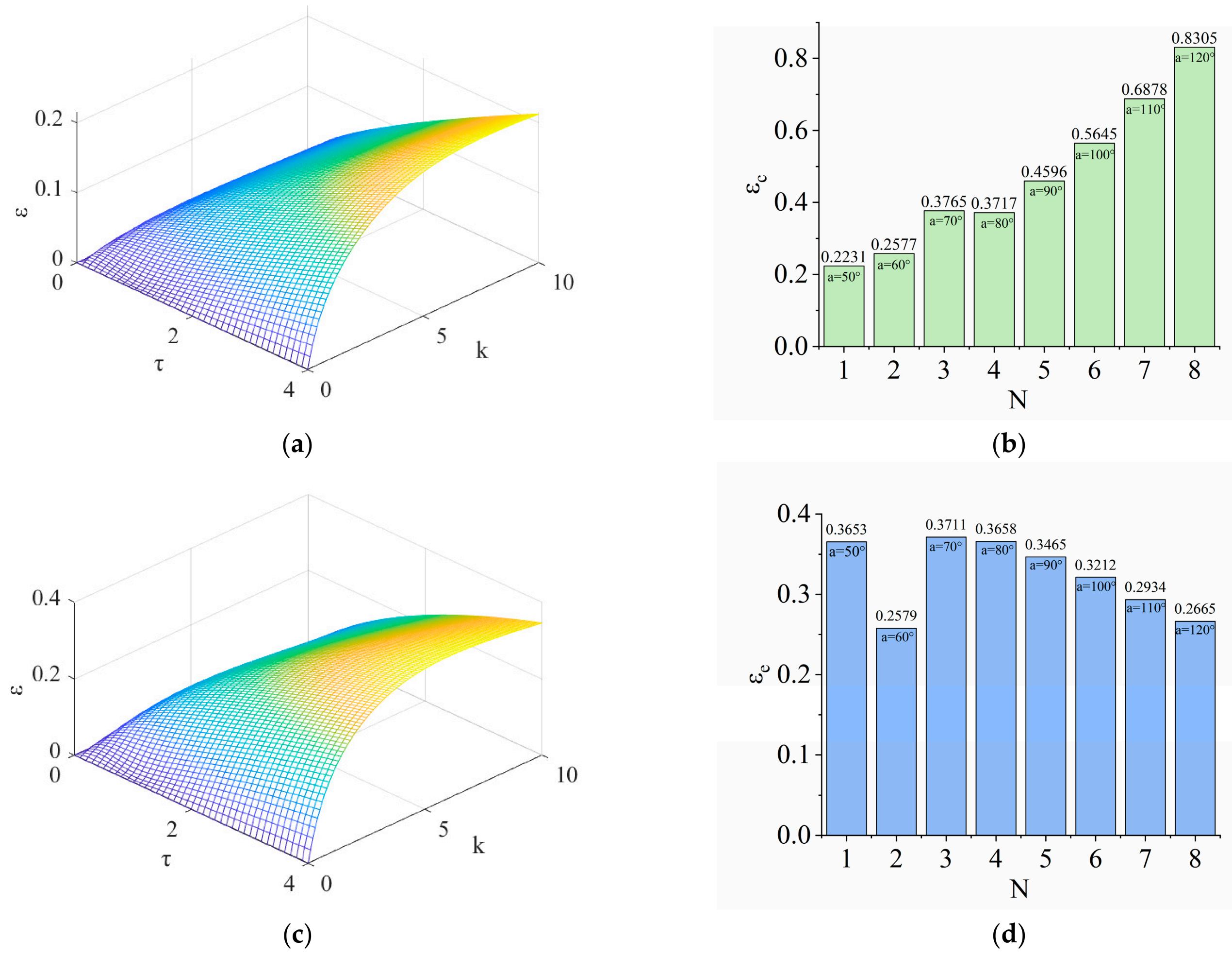

Figure 5. (**a**) $a = 70°$, $\chi = 1$ (the cooling mode). (**b**) Dimensionless cooling performance under various phase angles (the cooling mode). (**c**) $a = 70°$, $\chi = 1$ (the cooling mode). (**d**) Dimensionless cooling performance under various phase angles (the cooling mode).

With the increase in phase angle from 50° to 120°, ε_c rises more rapidly, owing to the improved coupling of thermodynamic processes; for example, ε_c increases from approximately 0.25 at $\alpha = 50°$ to about 0.65 at $\alpha = 120°$. The enhanced separation between the heat absorption and release stages drives the cycle closer to the ideal Stirling process, leading to a marked increase in the cooling effectiveness per unit time, as shown in Figure 5b.

The influence of temperature ratio and swept volume ratio on the dimensionless heating capacity exhibits a trend similar to that observed in cooling, as illustrated in Figure 5c.

With increasing phase angle, the dimensionless heating capacity initially exhibits slight fluctuations and then gradually decreases, with a local maximum occurring at 70°, as shown in Figure 5d.

At small phase angles, heat absorption at the hot end coincides with compression, yielding effective gas heat transfer and higher heating capacity. Excessively large phase angles disrupt this synchronization, reducing heat exchange efficiency and weakening heating performance. Cooling and heating modes require different optimal phase angles. Cooling favors larger phase angles due to improved separation of heat absorption and release, whereas heating relies on continuous heat release and pressure difference, making large phase angles less effective. The local maximum at 70° marks the best compromise for heating, beyond which its advantage declines.

3.3. Effect of the Swept Volume Ratio κ and Phase Angle α on the Dimensionless Work and the Nondimensional Heating/Cooling Capacity

With the increase in the swept volume ratio κ, ε_c, ε_e, Z_c, and Z_e exhibit a monotonic rise, while their growth rates gradually decline and eventually approach a plateau, as illustrated in Figure 6a. Both the dimensionless cooling capacity ε_c and heating capacity εe increase with the swept volume ratio κ, but ε_e remains consistently higher than ε_c over the entire range. As κ increases from 1 to 6, ε_c rises from approximately 0.03 to 0.07, while ε_e increases from approximately 0.08 to 0.18. Accordingly, the difference between ε_e and ε_c increases from about 0.05 to nearly 0.11, indicating that the heating performance is more sensitive to the swept volume ratio than the cooling performance. Z_c and Z_e exhibit coincident curves with identical values, increasing from around 0.01 to 0.05 as κ rises from 1 to 6, demonstrating that the dimensionless work is invariant between cooling and heating modes. This invariance stems from the fact that work transfer depends on piston dynamics and gas compression/expansion, rather than on the direction of heat flow.

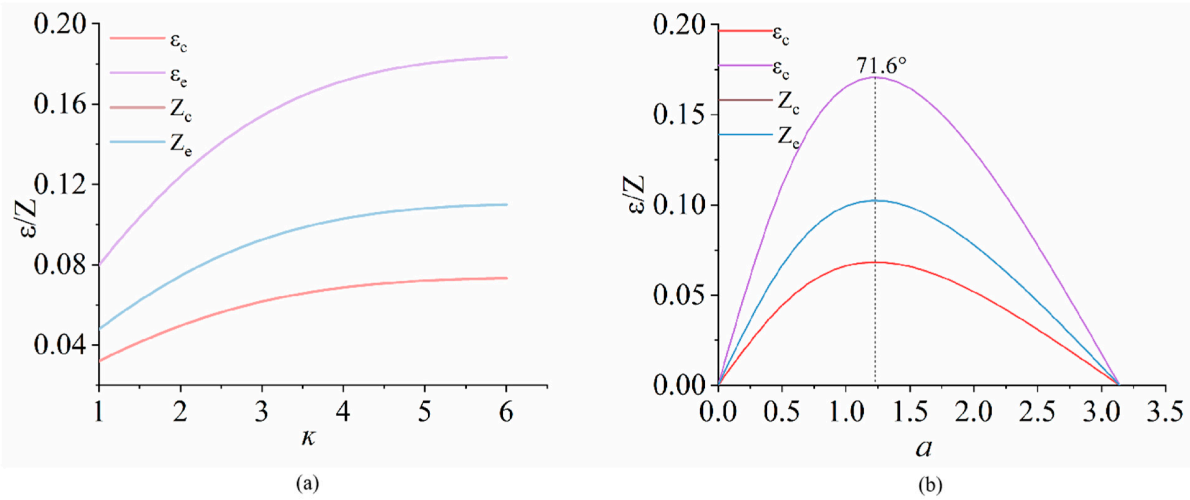

Figure 6. (**a**) Effect of the swept volume ratio κ on the dimensionless work Z and the nondimensional cooling/heating performance (χ = 1). (**b**) Influence of phase angle α on dimensionless work and cooling/heating performance (χ = 1).

With the increase in phase angle α, ε_c, ε_e, Z_c, and Z_e exhibit a unimodal trend, first increasing and then decreasing, as shown in Figure 6b. For small α ($\alpha < 30°$), limited gas displacement between the chambers causes inadequate heat transfer, yielding low ε and Z (ε_c and ε_e below 0.05, Z below 0.02). With increasing α, the staggered compression–expansion improves heat transfer separation, bringing the cycle closer to the ideal Stirling cycle and rapidly enhancing cooling/heating performance and dimensionless work. When α exceeds a critical value ($a > 90°$), the synergistic effect of thermodynamic processes between the chambers weakens, causing ε and Z to decrease. ε_e consistently exceeds ε_c, reaching the largest difference at the peaks, which suggests that the heating cycle outperforms the cooling cycle in energy output under identical phase angle conditions. At $\alpha \approx 71.6°$, ε_e peaks at 0.18, while ε_c reaches only 0.07, highlighting the stronger sensitivity of the heating cycle to the phase angle. Near $\alpha = 71.6°$, Z reaches a maximum of approximately 0.10, indicating that the energy conversion efficiency is optimal at this phase angle. For very small or large α ($\alpha < 20°$ or $\alpha > 120°$), overlapping heat transfer between the chambers disrupts the thermodynamic processes, causing deviations from the ideal Stirling cycle and a decline in performance. At $\alpha \approx 71.6°$, optimal temporal phasing between expansion chamber heat absorption and compression chamber heat rejection maximizes cycle independence, resulting in simultaneous peaks of ε and Z.

3.4. Influence of Piston Phase Angle α on p–v Diagrams

The thermodynamic processes introduced in Figure 1c are further quantified using the *p*–*v* indicator diagrams shown in Figure 7. The enclosed area of the *p*–*v* loop represents the net work output of one thermodynamic cycle. Therefore, the evolution of the *p*–*v* diagram with piston phase angle provides direct insight into the degree of matching between the compression and expansion processes. Figure 7 illustrates the influence of the piston phase angle on the *p*–*v* cycle. The enclosed area represents the net work produced during one thermodynamic cycle. As the phase angle increases, the cycle area first enlarges and then decreases, reaching its maximum at approximately 75°. At a phase angle of approximately 75°, the cycle area approaches its maximum, indicating that the time shift between heat absorption in the expansion chamber and heat release in the compression chamber is most favorable, leading to near-optimal heat transfer. As the phase angle increases to 90°, although it approaches the theoretically ideal value, the actual cycle area becomes smaller than that at 75°, suggesting that the coupling between heat transfer and gas compression–expansion remains suboptimal.

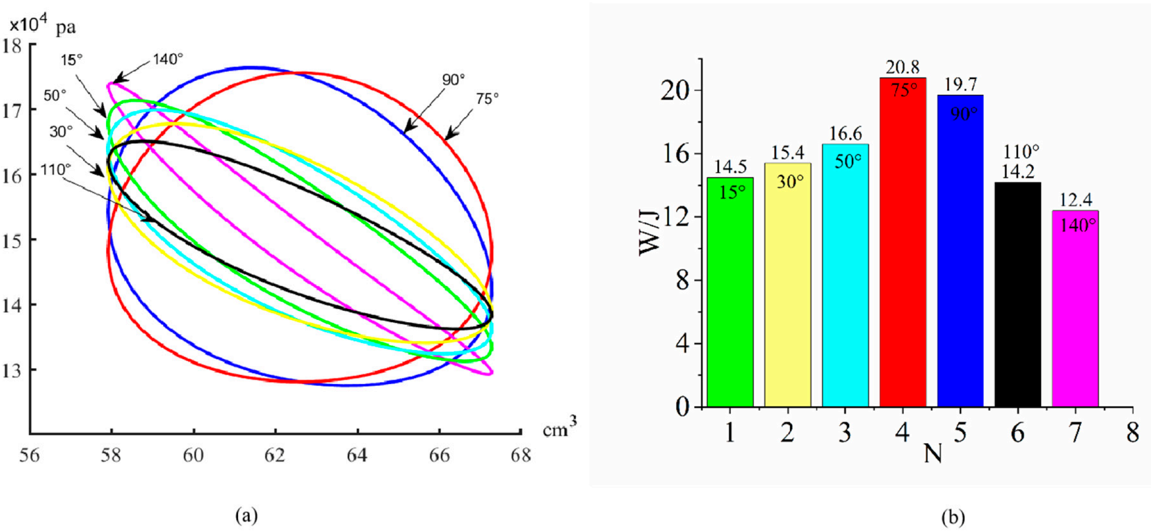

Figure 7. (**a**) *p*–*v* indicator diagrams (χ = 1). (**b**) Areas of *p*–*v* indicator diagrams.

To assess the reliability of the present model, the predicted trends are compared with previously reported experimental and numerical results from recent studies on free-piston Stirling coolers [27–30]. It is found that the unimodal dependence of performance on phase angle is consistent with experimental observations, and the saturation behavior at large swept volumes agrees with CFD-based studies. Quantitative discrepancies (20–40%) are expected due to neglected losses.

3.5. Model Validation and Comparison

To evaluate the reliability of the present dimensionless model, the predicted trends are compared with those reported in previous experimental and numerical studies on free-piston Stirling coolers [31,32].

First, the unimodal dependence of cooling/heating performance on phase angle is consistent with experimental observations, where optimal performance typically occurs within 60–90°. This agreement confirms that the model captures the essential phase coupling mechanism.

Second, the saturation behavior observed at large swept volume ratios (κ > 6) aligns with CFD-based studies, which attribute this phenomenon to flow resistance and limited heat exchanger effectiveness.

However, quantitative discrepancies are expected. Compared with adiabatic or CFD models, the present isothermal model tends to overpredict performance by approximately 20–40%, primarily due to:

(i) Neglect of regenerator inefficiency.
(ii) Absence of pressure drop.
(iii) Omission of shuttle heat transfer losses.

Furthermore, practical systems often operate at lower temperature ratios ($\tau \approx 1.2$–1.5), whereas the present model predicts higher performance at larger τ values. This difference reflects the increasing irreversibility at high temperature ratios, which is not captured in the idealized framework.

Overall, despite its limitations, the present model provides physically consistent trends and valuable insights into multi-parameter coupling mechanisms, serving as a theoretical upper bound for system performance.

3.6. CFD Validation of the Thermodynamic Model

To further evaluate the reliability of the present dimensionless model, a comparative analysis is conducted with computational fluid dynamics (CFD) results reported in the recent literature on free-piston Stirling systems [20,32].

In CFD simulations, the governing equations of mass, momentum, and energy conservation are solved with consideration of real-gas effects, viscous dissipation, pressure drop, and regenerator heat transfer inefficiency. These factors are neglected in the present Schmidt-based isothermal model, leading to expected discrepancies in quantitative results.

Figure 8 compares the variation in dimensionless cooling capacity ε_c with phase angle α obtained from the present model and CFD-based studies. Both the present model and CFD-based results exhibit a consistent unimodal variation in ε_c with phase angle α, with the optimal range located between 60° and 90°.

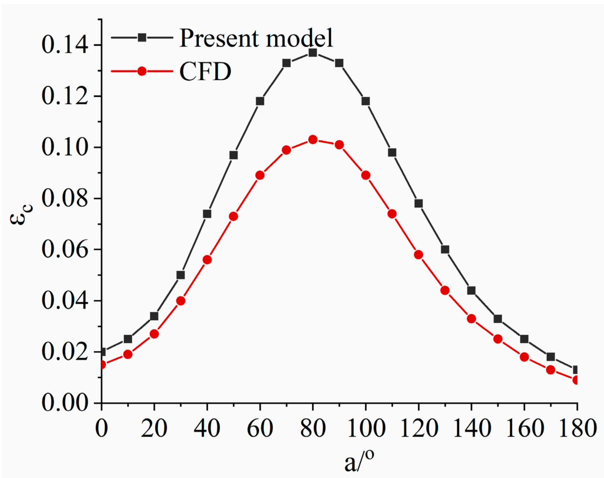

Figure 8. Comparison of dimensionless cooling capacity ε_c versus phase angle α between present model and CFD results.

However, the magnitude of ε_c predicted by the present model is generally higher than that obtained from CFD simulations. For example, at $\alpha \approx 70°$, the present model predicts $\varepsilon_c \approx 0.12$, whereas CFD results typically range between 0.08 and 0.10, indicating an overestimation of approximately 20–30%.

This discrepancy can be attributed to several factors:

(i) The neglect of regenerator inefficiency and axial conduction losses.
(ii) The absence of pressure drop across heat exchangers.

(iii) The idealized assumption of isothermal processes.
(iv) Simplified sinusoidal piston motion.

Figure 9 further presents the comparison of dimensionless work Z as a function of swept volume ratio κ. Both the present model and CFD results demonstrate a monotonic increase followed by saturation behavior, confirming that the model captures the essential mechanism of diminishing performance gain at large κ. Both the present model and CFD results demonstrate a monotonic increase followed by saturation behavior, confirming that the model captures the essential mechanism of diminishing performance gain at large κ.

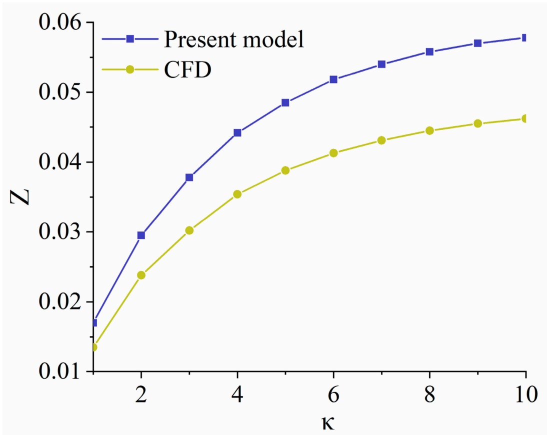

Figure 9. Further presents the comparison of dimensionless work Z as a function of swept volume ratio κ.

The agreement in trend between the present model and CFD results indicates that the dominant thermodynamic mechanisms, such as phase-dependent heat transfer separation and volumetric efficiency, are well captured by the simplified analytical framework. In particular, the unimodal dependence on phase angle reflects the competition between process synchronization and thermodynamic irreversibility. At moderate phase angles, the separation between compression and expansion processes is optimized, maximizing effective heat transfer. At larger phase angles, however, excessive phase lag weakens pressure–volume coupling, reducing cycle efficiency. The saturation behavior at large swept volume ratios is primarily associated with flow resistance and limited heat exchanger effectiveness, which become increasingly significant in CFD simulations but are not included in the present model.

Overall, although the present model overpredicts the absolute performance values, it provides accurate predictions of performance trends and parameter sensitivity. Therefore, it can be considered a theoretical upper-bound model, which is valuable for preliminary design and parameter optimization.

From the perspective of practical air conditioner performance, the dimensionless cooling capacity employed in the present study provides a direct measure of the thermodynamic cooling potential under the ideal Schmidt assumptions. Since the classical Schmidt model neglects pressure losses, mechanical friction, regenerator inefficiency, and other irreversible effects, it cannot accurately predict the actual COP of a practical free-piston Stirling air conditioner. Nevertheless, the variations in the dimensionless cooling capacity with temperature ratio, swept volume ratio, dead volume ratio, and phase angle provide valuable insight into the relative influence of these design parameters on the system cooling capability. Therefore, the present results can be regarded as theoretical upper-bound performance references for preliminary parameter selection, whereas quantitative COP evaluation requires non-ideal thermodynamic modeling and experimental validation, which will be considered in future work.

3.7. Model Limitations and Error Analysis

The present study is based on the classical Schmidt isothermal model, which provides an analytical framework for evaluating the thermodynamic characteristics of free-piston Stirling air conditioners under ideal assumptions. Although this model is widely adopted for preliminary thermodynamic analysis, several assumptions inevitably introduce deviations from practical operating conditions. First, the regenerator is assumed to operate ideally with perfect heat regeneration. In practical Stirling systems, the regenerator effectiveness is typically lower than unity because of finite heat transfer coefficients, flow maldistribution, axial heat conduction, and matrix thermal inertia. Consequently, part of the thermal energy cannot be effectively recovered, resulting in lower cooling and heating capacities than those predicted by the present model. Second, pressure losses throughout the heater, regenerator, cooler, and connecting passages are neglected. In practical systems, oscillating flow through porous regenerators and narrow channels inevitably generates pressure drops, reducing the effective pressure amplitude and consequently decreasing the cycle work and thermodynamic performance. Therefore, the present results should be interpreted as theoretical upper-bound predictions under ideal Schmidt assumptions.

4. Conclusions

Based on the ideal isothermal Schmidt model, this study systematically analyzed and optimized the key thermodynamic parameters of a free-piston Stirling air conditioning system using the Schmidt dimensionless analysis method. Therefore, the conclusions presented in this study are applicable to ideal thermodynamic conditions and provide theoretical guidance for preliminary parameter selection rather than direct engineering design recommendations.

The dimensionless cooling capacity is strongly affected by the temperature ratio τ, swept volume ratio κ, and dead volume ratio χ. The maximum dimensionless cooling capacity (ε_c = 0.1696) is achieved at a high temperature ratio (τ = 3) and large swept volume ratio (χ = 1), whereas the optimal heating performance (ε_h = 0.1032) occurs at a lower temperature ratio (τ = 1.5) with minimal dead volume (χ = 1). The difference originates from the thermodynamic nature of each mode: cooling benefits from greater temperature differences and displacement volume, while heating efficiency is enhanced by a moderated temperature gradient. These findings emphasize the necessity of mode-specific parameter optimization in Stirling system design.

At a fixed phase angle, increasing the dead volume ratio χ results in a significant decrease in the dimensionless cooling capacity, whereas enlarging the phase angle α from 50° to 120° markedly enhances it, elevating the dimensionless cooling capacity ε_c from approximately 0.25 to 0.65 due to optimized thermodynamic process coupling. The sensitivity of cooling capacity to the swept volume ratio κ is highly dependent on the temperature ratio τ, with the two parameters exhibiting a nonlinear synergistic effect; performance saturation occurs at $\tau > 3$ and $\kappa > 6$. Although its impact is comparatively weaker, the dead volume ratio remains non-negligible. Consequently, an optimal design must strike a balance between the dead volume and swept volume. Within the framework of the ideal Schmidt model, medium-to-high temperature ratios ($\tau \approx$ 3–4) combined with moderate swept volume ratios ($\kappa \approx$ 6–8) are identified as favorable parameter combinations that provide a good compromise between thermodynamic performance and structural compactness. It should be emphasized that these values represent theoretical optima under ideal assumptions and require further validation using non-ideal thermodynamic models and experimental investigations before being adopted for practical engineering applications.

With a constant dead volume, the dimensionless heating capacity diminishes as the temperature ratio increases. At a fixed temperature ratio, increasing the dead volume similarly reduces heating performance. As the swept volume ratio increases from 1 to 6, the heating capacity ε_e exhibits a monotonic rise from a low value to approximately 0.20, yet the performance gain saturates beyond $\kappa > 4$. Optimal heating occurs at phase differences between 70° and 80°, with the peak performance being highly sensitive to this parameter. Specifically, at $\alpha \approx 71.6°$, ε_e reaches its maximum value of 0.18, significantly higher than the corresponding cooling capacity ($\varepsilon_c \approx 0.07$) at the same angle, underscoring the heating cycle's superior energy output. Furthermore, larger dead volumes generally limit the heating gain, and the enhancing effect of the swept volume ratio becomes less pronounced at elevated temperature ratios, as the system's performance progressively approaches a plateau.

The *p*–*v* diagram cycle area reveals a non-monotonic relationship between the system work output and phase angle: as the phase angle increases from 15° to 75°, the cycle area expands significantly from 14.4 to 20.8, representing a 44.4% increase, indicating optimal thermodynamic process matching. However, beyond 75°, the area decreases sharply, dropping to 12.4 at 140°—a 40.4% reduction from the peak value. This decline is attributed to deteriorated process coupling at excessive phase angles, which substantially reduces output efficiency. Thus, a phase angle of approximately 75° is identified as optimal for maximizing work output.

It should be noted that the present study is based on the ideal Schmidt isothermal model, in which pressure losses, heat transfer limitations, mechanical friction, gas leakage, and other irreversible effects are neglected. Therefore, the optimal parameter ranges reported in this work should be interpreted as theoretical references under ideal operating conditions. Future work will incorporate non-ideal thermodynamic effects and experimental validation to further assess the applicability of these parameter combinations in practical free-piston Stirling air conditioning systems.

Although the present Schmidt-based dimensionless analysis does not directly evaluate the actual system COP, the identified parameter trends provide theoretical guidance for improving cooling performance and establishing a foundation for future COP prediction based on non-ideal thermodynamic and dynamic models. It should be noted that the performance saturation observed at large κ and τ is obtained under the assumptions of the ideal Schmidt model. In practical free-piston Stirling air conditioners, further performance improvement would be limited by irreversibilities such as pressure loss, regenerator inefficiency, shuttle heat transfer, gas leakage, and finite-rate heat transfer. These irreversible effects increase exergy destruction and reduce the effective cooling/heating capacity, especially under large swept volume ratios and high temperature ratios. Therefore, the present results should be interpreted as theoretical upper-bound predictions. A quantitative exergy loss analysis based on a non-ideal thermodynamic model will be conducted in future work. From a multi-objective perspective, the optimal parameter combination for cooling does not necessarily coincide with that for heating. Cooling performance benefits from a relatively high temperature ratio and an increased swept volume ratio, whereas heating performance is more sensitive to phase matching and dead volume reduction. Therefore, a balanced design should avoid pursuing the maximum cooling or heating capacity alone. Under the ideal Schmidt assumptions, a moderate swept volume ratio, a relatively small dead volume ratio, and an appropriate phase angle provide a reasonable compromise between cooling capacity, heating capacity, and cycle work. A rigorous multi-objective optimization considering practical constraints, irreversible losses, and system COP will be carried out in future work.

Author Contributions: Conceptualization, methodology, formal analysis, Y.W. (Yajuan Wang); software, Y.W. (Yuehong Wang); methodology, G.Z.; Validation, J.G.; Validation, X.L. All authors have read and agreed to the published version of the manuscript.

Funding: This research was supported by the Shaanxi Province's Key Research and Development Program (General Projects), 2024GX-YBXM-253; Science and Technology Innovation Talent Program of Xianyang, L2024-CXNL-KJRCTD-KJRC-0013; Special Project for Innovation Capacity Support Plan–Scientific and Technological Innovation Team, S2025-CXNL-KJTD-4243.

Data Availability Statement: Data will be available on request from the authors.

Conflicts of Interest: The authors declare no conflicts of interest.

Abbreviations

a	piston phase angle
p	pressure
ε	dimensionless capacity
τ	temperature ratio
ω	angular frequency
θ_1	the minimum
W	the cycle work
κ	sweep volume ratio
χ	dead volume ratio
v	volume
t	time
γ	pressure ratio
Q	quality of heat
Z	dimensionless work
Greek Symbols	
e	expansion
T	working volume
min	minimum
c	compression
h	heating
max	maximum

Appendix A

Based on the Schmidt isothermal model, the instantaneous volumes of the expansion and compression chambers are expressed as:

$$\begin{cases} V_c = V_{c0} + \frac{V_c}{2}(1 + \cos(\omega t - \alpha)) \\ V_e = V_{e0} + \frac{V_e}{2}(1 + \cos(\omega t + \alpha)) \end{cases} \tag{A1}$$

where ω is the angular frequency and α is the phase angle.

For the free-piston Stirling system, the condition of minimum compression volume is used as a reference state. At this instant, the rate of change in compression volume satisfies:

$$dV_c/dt = 0 \tag{A2}$$

Taking the derivative of V_c with respect to time:

$$dV_c/dt = -(V_c/2)\omega sin(\omega t - a) \tag{A3}$$

Thus:

$$\sin(\omega t - \alpha) = 0 \tag{A4}$$

which leads to:

$$\omega t = a + n\pi \tag{A5}$$

Substituting into the trigonometric relationships, the sine and cosine terms can be expressed as functions of α and θ_1:

$$\begin{cases} \sin(\omega t) = \sin(\alpha + \theta_1) \\ cos(\omega t) = \sin(\alpha + \theta_1) \end{cases} \tag{A6}$$

Under the assumption of instantaneous pressure equilibrium and ideal gas behavior, the total mass conservation yields:

$$p(t) = mR/(V_e/T_e + V_c/T_c + V_r/T_r) \tag{A7}$$

where V_r is the regenerator volume.

Introducing the temperature ratio $\tau = T_c/T_e$ and dead volume ratio χ, the denominator can be normalized:

$$p(t) = p_{mean}/[1 + A\cos(\omega t) + B\sin(\omega t)] \tag{A8}$$

where A and B are functions of τ, κ, and χ.

By defining:

$$\chi = \omega t - \theta_1 \tag{A9}$$

the pressure expression can be rearranged into harmonic form:

$$p(t) = p_{mean}/[1 + C\cos(x)] \tag{A10}$$

where C is the pressure amplitude coefficient.

Finally, the maximum and minimum pressures are obtained as:

$$\begin{cases} p_{\max} = p_{mean}(1 + C) \\ p_{\min} = p_{mean}(1 - C) \end{cases} \tag{A11}$$

thus, the pressure ratio is:

$$\gamma = p_{\max}/p_{\min} = (1 + C)/(1 - C) \tag{A12}$$

This completes the derivation from Equation (2) to Equation (6).

References

1. Getie, M.Z.; Lanzetta, F.; Bégot, S.; Admass, B.T.; Hassen, A.A. Reversed regenerative Stirling cycle machine for refrigeration application: A review. *Int. J. Refrig.* **2020**, *118*, 173–187. [CrossRef]
2. Abedrabboh, O.; Koç, M.; Biçer, Y. Sustainability performance of space-cooling technologies and approaches. *Energy Sources Part A Recovery Util. Environ. Eff.* **2022**, *44*, 9017–9042.
3. Wang, Y.; Guo, J. Influence of Dead Volume Ration on the Thermodynamic Performance of Free-Piston Stirling Machines. *Modelling* **2025**, *6*, 150. [CrossRef]
4. Wang, Y.; Zhang, J.; Guo, J.; Zhang, G.; Zhang, J. Performance Simulation and Experimental Verification of a Low-Temperature Differential Free-Piston Stirling Air Conditioner Under Multi-Harmonic Drive. *Processes* **2025**, *13*, 134. [CrossRef]
5. Zare, S.; Tavakolpour-Saleh, A.R. Free piston Stirling engines: A Review. *Int. J. Energy Res.* **2020**, *44*, 5039–5070.
6. Goetzler, W.; Guernsey, M.; Young, J.; Fuhrman, J.; Abdelaziz, O. *The Future of Air Conditioning for Buildings*; Navigant Consulting: Burlington, MA, USA, 2016.
7. Formosa, F.; Despesse, G. Analytical model for Stirling cycle machine Design. *Energy Convers. Manag.* **2010**, *51*, 1855–1863. [CrossRef]
8. Organ, A.J. *The Regenerator and the Stirling Engine*; Office of Scientific and Technical Information: Oak Ridge, TN, USA, 1997.
9. Marciniak, T.J.; Bratis, J.C.; Davis, A.; Lee, C. *Assessment of Stirling Engine Potential in Total and Integrated Energy Systems*; Argonne National Laboratory (ANL): Argonne, IL, USA, 1979.

10. Gao, X.Q.; Shen, J.; He, X.N.; Tang, C.; Li, K.; Dai, W.; Li, Z.X.; Jia, J.C.; Gong, M.Q.; Wu, J.F. Improvements of a room-temperature magnetic refrigerator combined with Stirling cycle refrigeration effect. *Int. J. Refrig.* **2016**, *67*, 330–335. [CrossRef]
11. Raghavendra, H.; Suryanarayana, P.R.; Hemachandra, R.K. Effect of geometric and operational parameters on the performance of a beta-type Stirling engine: A numerical study. *Iran. J. Sci. Technol. Trans. Mech. Eng.* **2022**, *46*, 1–13. [CrossRef]
12. Senft, J.R. *Mechanical Efficiency of Heat Engines*; Cambridge University Press: Cambridge, UK, 2007.
13. Wu, F.; Chen, L.G.; Sun, F.R.; Yu, J. *Finite Time Thermodynamic Optimization for Stirling Machines*; Chemical Industry Press: Beijing, China, 2008.
14. Wen, H.; Long, D.; Shao, Y.; Shuai, Z. Design and multi-objective optimization of a tubular linear PM machine for Stirling generator based on gradient boosting regression tree surrogate model. *IEEE Trans. Energy Convers.* **2024**, *40*, 1655–1665. [CrossRef]
15. Chen, P.; Zhong, G.; Niu, Y.; Liu, Y. Performance optimization of a free piston stirling engine using multi-section regenerators based on the response surface methodology. *Energy* **2022**, *261*, 125221. [CrossRef]
16. Chen, P.; Deng, C.; Luo, X.; Ye, W.; Hu, L.; Wang, X.; Liu, Y. Performance optimization of a free piston Stirling engine using the self-directed online machine learning optimization approach. *Appl. Therm. Eng.* **2024**, *236*, 121482. [CrossRef]
17. Ye, W.; Wang, X.; Liu, Y.; Chen, J. Analysis and prediction of the performance of free-piston Stirling engine using response surface methodology and artificial neural network. *Appl. Therm. Eng.* **2021**, *188*, 116557. [CrossRef]
18. Kong, L.; Li, J.; Wu, Z.; Sun, S. Parametric Study on the Performance of Gas Springs in FPSE With Pneumatic Supporting System. *Energy Sci. Eng.* **2025**, *13*, 4059–4086. [CrossRef]
19. Luo, X.; Wang, X.; Yan, C.; Zhang, A.; Zhang, X.; Ye, W. Performance prediction and parametric optimization of γ-type free piston Stirling engine. *Therm. Sci.* **2024**, *28*, 269–281. [CrossRef]
20. Ye, W.; Wang, W.; Long, H.; Sun, S.; Kong, L. Effect of thermodynamic-dynamic parameters on the oscillation and performance of a free piston Stirling engine. *Appl. Therm. Eng.* **2024**, *253*, 123845. [CrossRef]
21. Bataineh, K. Hybrid fuel-assisted solar-powered Stirling engine for combined cooling, heating, and power systems: A review. *Energy* **2024**, *300*, 131506. [CrossRef]
22. Urieli, I.; Berchowitz, D. *Stirling Cycle Engine Analysis*; Office of Scientific and Technical Information: Oak Ridge, TN, USA, 1983.
23. Zare, S.; Tavakolpour-Saleh, A.R.; Aghahosseini, A.; Sangdani, M.H.; Mirshekari, R. Design and optimization of Stirling engines using soft computing methods: A review. *Appl. Energy* **2021**, *283*, 116258. [CrossRef]
24. Demeke, W.; Ryu, B.; Ryu, S. Machine learning-based optimization of segmented thermoelectric power generators using temperature-dependent performance properties. *Appl. Energy* **2024**, *355*, 122216. [CrossRef]
25. Bitsikas, P.; Rogdakis, E.; Dogkas, G. CFD study of heat transfer in Stirling engine regenerator. *Therm. Sci. Eng. Progress.* **2020**, *17*, 100492. [CrossRef]
26. Wong, H.M.; Bahar, R.; Ong, Y.S. Experimental evaluation of the displacer and working piston hybrid motion to improve the performance of a Stirling engine. *Appl. Therm. Eng.* **2025**, *279*, 127936. [CrossRef]
27. Muhammad, S.; Zhang, X.Q. Parametric study of miniature Stirling cryocooler for high temperature infrared detector with design refinement for SWaP configuration. *Appl. Therm. Eng.* **2025**, *273*, 126495. [CrossRef]
28. Wang, H.T.; Chen, Y.Y.; Luo, E.C.; Kang, H.F.; Zhu, S.M. Study on the influence of real gas compressibility on the performance of free-piston Stirling engines. *Appl. Therm. Eng.* **2025**, *280*, 128441. [CrossRef]
29. Chai, J.; Yang, X.H.; Gao, X.Y.; Zhang, X.Y.; Li, C.H. Effects of thermodynamic parameters on thermoacoustic characteristics of free-piston Stirling engine. *Appl. Therm. Eng.* **2025**, *269*, 126181. [CrossRef]
30. Zhou, Q.; Chen, Y.C.; Sheng, S.J.; Wang, Y.K.; He, T.B.; Jin, T. Experimental study on a wet thermoacoustic Stirling engine for water pumping. *Appl. Therm. Eng.* **2025**, *265*, 125558. [CrossRef]
31. Yang, H.S.; Kuan, S.Y.; Ali, M.A. Effect of dynamic characteristics on the performance of a free-piston Stirling heat-driven cooler. *Appl. Therm. Eng.* **2025**, *274*, 26795. [CrossRef]
32. Xiao, G.; Sultan, U.; Ni, M.J.; Peng, H.; Zhou, X.; Wang, S.L.; Luo, Z.Y. Design optimization with computational fluid dynamic analysis of β-type Stirling engine. *Appl. Therm. Eng.* **2017**, *113*, 87–102. [CrossRef]

Disclaimer/Publisher's Note: The statements, opinions and data contained in all publications are solely those of the individual author(s) and contributor(s) and not of MDPI and/or the editor(s). MDPI and/or the editor(s) disclaim responsibility for any injury to people or property resulting from any ideas, methods, instructions or products referred to in the content.